Radio Science, Volume 16, Number 1, pages 93–100, January–February 1981

Ocean surface current measurements by an *L* band two-frequency microwave scatterometer

Werner Alpers

Institut für Geophysik, Universität Hamburg, and Max Planck Institut für Meteorologie, Hamburg, Federal Republic of Germany

Jens Schröter

Max Planck Institute für Meteorologie, Hamburg, Federal Republic of Germany

Franz Schlude and Hans-Jürgen Müller

Institut für Hochfrequenztechnik, Deutsche Forschungs- und Versuchsanstalt für Luft- und Raumfahrt, Oberpfaffenhofen, Federal Republic of Germany

Klaus Peter Koltermann

Deutsches Hydrographisches Institut, Hamburg, Federal Republic of Germany

(Received April 30, 1980; revised August 14, 1980; accepted August 14, 1980.)

Real time current measurements with an *L* band pulsed two-frequency microwave scatterometer (2FS) were carried out from the German North Sea Research Platform (Forschungsplattform Nordsee) during the 1979 Marine Remote Sensing (Marsen) experiment. The principle of this remote sensing technique consists of measuring the phase velocity of a long ocean wave by resonant scattering of a beat wave produced by two microwave signals. The difference between the measured phase velocity and the phase velocity, as calculated from the dispersion relation for still water, represents a weighted average of the ocean current near the surface. Current measurements over full tidal cycles in various wind conditions (up to 18 m s^{-1}) are presented. At high wind speeds, pronounced differences are found between the 2FS measurements and the in situ current measurements made at depths of 9 m and 23 m. These differences can be explained as the effect of the wind stress acting on the upper layer of the ocean. The measurements indicate that the interaction of the tide- and wind-driven currents strongly depends on the parallel and antiparallel orientation of the currents. The accuracy of the measurements reported here is approximately ±0.12 m s^{-1}, but this can, in principle, be improved.

1. INTRODUCTION

In situ measurements of near-surface currents by conventional current meters are difficult to perform, because they are strongly effected by wave motions. Knowledge of near-surface currents is very valuable in the study of many problems, for example, in studies of the interaction of the wind-driven current with the tidal current, the build-up of storm surges, or the transport of floating matter (oil spills). Alternative remote sensing techniques are therefore being considered in order to obtain these measurements. Only two techniques, the HF technique and the two-frequency microwave technique, have been deployed. In both techniques, the surface current information is obtained by measuring the phase velocity c_{ph} of long ocean waves. In the presence of surface currents the actual phase velocity differs from the phase velocity calculated from the still water dispersion relation. The difference between the measured and calculated phase velocity, $c_{ph} - c_{ph}^{0}$, yields a weighted average of the surface current of the upper few meters of the ocean.

The phase velocity of long ocean waves can be measured by means of Bragg scattering, with electromagnetic waves in the decameter-wavelength range (HF waves). Currently, much research is being devoted to developing such HF techniques for measuring surface currents in coastal waters [*Stewart and Joy*, 1974; *Teague et al.*, 1977; *Barrick et al.*, 1977; *Ha*, 1979].

Paper number 80S1178.
0048-6604/81/0102-1178$01.00

The two-frequency microwave technique is an alternative for measuring surface currents via the phase velocity of long ocean waves. It exploits the fact that the Bragg backscattering of microwaves, which is caused by scattering at short ocean surface waves with wavelengths in the centimeter/decimeter range (ripple waves), is modulated by the long ocean waves. To measure this modulation, the two-frequency microwave technique employs nonlinear signal detection. The phase velocity of the long ocean waves is determined from the statistical analysis of the fourth-order moments of the backscattered amplitudes [*Plant,* 1977; *Alpers and Hasselmann,* 1978].

Using a continuous wave (CW) X band radar, *Schuler* [1978] has experimentally demonstrated that two-frequency microwave scattering is indeed sensitive to ocean surface currents.

In this paper, we present experimental results of surface current measurements obtained with the aid of an L band pulsed two-frequency scatterometer during the 1979 Marsen experiment in the North Sea. The scatterometer was installed on the German North Sea Research Platform, which is situated approximately 70 km west of the island of Sylt (Germany). Surface current measurements were made over full tidal cycles for low- and high-wind conditions and were compared with in situ current measurements at 9-m and 23-m depths. On several occasions, pronounced differences were found between the currents measured by the 2FS and the in situ current meters. These differences are not unexpected, since the 2FS senses the current in the upper few meters of the ocean, which is more strongly exposed to the action of the wind than to the deeper layers of the ocean. The measurements clearly demonstrate that the two-frequency microwave scatterometer is a powerful research tool for studying the transfer of momentum across the air-sea interface and the momentum balance in the ocean.

2. THEORY

Consider a microwave scatterometer (2FS) that emits successive pairs of pulses at two slightly different frequencies f_1 and f_2. The time interval between subsequent pulses with frequencies f_1 and f_2 must be so small that the change in scattering geometry is negligible. In this case, phase differences in the backscattered signals are due only to the frequency separation between the two pulses.

Let B_1 and B_2 denote the (complex) amplitudes of the backscattered signals that originate from the pulses with frequencies f_1 and f_2, respectively. The two-frequency method consists of calculating the Doppler spectrum of the product signal $B_1 \cdot B_2^*$, where the asterisk denotes complex conjugation. The modulation of the Bragg scattering waves by the surface waves results in two peaks of the Doppler spectrum [*Alpers and Hasselmann,* 1978] at

$$\omega = \pm\hat{\omega} + 2\Delta\mathbf{k} \cdot \mathbf{v} \tag{1}$$

where $\Delta\mathbf{k}$ is the projection of $\mathbf{k}_2 - \mathbf{k}_1$ on to the horizontal plane; $\mathbf{k}_1$ and $\mathbf{k}_2$ are the three-dimensional wave number vectors of the emitted radar pulses of frequencies f_1 and f_2, respectively; $|\mathbf{k}_1| = (2\pi/c)f_1$; $|\mathbf{k}_2| = (2\pi/c)f_2$; and c is the speed of light. The radian frequency $\hat{\omega}$ of the resonant water wave is related to the resonant wave number $\hat{\mathbf{k}}$ by the dispersion relation for still water:

$$\hat{\omega} = [g|\hat{\mathbf{k}}| \tanh (|\hat{\mathbf{k}}|\, d)]^{1/2} \tag{2}$$

where g is the acceleration of gravity, and d is the water depth; $\hat{\mathbf{k}}$ is given by the Bragg resonance condition for the 'beat wave' with wave number $\mathbf{k}_2 - \mathbf{k}_1$:

$$\hat{\mathbf{k}} = \pm 2\Delta\mathbf{k} \tag{3}$$

Expressed in terms of ocean wavelength $\hat{\lambda}$ ($\hat{\lambda} = 2\pi|\hat{\mathbf{k}}|^{-1}$), beat frequency $\Delta f = f_2 - f_1$, and depression angle θ, the Bragg resonance condition for the beat wave reads

$$\hat{\lambda} = \frac{150}{\Delta f}\frac{1}{\cos\theta} \tag{4}$$

where the units of $\hat{\lambda}$ are meters and those of Δf are Megahertz. Finally, $\mathbf{v}$ denotes a weighted mean current of the upper layer of the ocean (the weighting function is proportional to $e^{-2|\hat{\mathbf{k}}|z}$, where z is the depth below the surface (see (6)). In general, $\mathbf{v}$ is a superposition of the tidal current $\mathbf{v}^t$, other currents associated with mean ocean circulation $\mathbf{v}^{oc}$, the wind drift $\mathbf{v}^d$, and wave-induced currents $\mathbf{v}^{nl}$:

$$\mathbf{v} = \mathbf{v}^t + \mathbf{v}^{oc} + \mathbf{v}^d + \mathbf{v}^{nl} \tag{5}$$

The wind drift $\mathbf{v}^d$ and mean ocean circulation $\mathbf{v}^{oc}$ cannot always be rigorously separated, but here we regard $\mathbf{v}^d$ as the current in the upper layer of the ocean that is driven by the local wind stress

(the 'Ekman layer'), as opposed to the deeper current field $\mathbf{v}^{oc}$ that is driven by the density field.

The wave-induced current includes the well-known Stokes drift [see, e.g., *Phillips,* 1966], as well as corrections of the phase velocity originating from nonlinear wave-wave interaction processes, which have been calculated by *Longuet-Higgins and Phillips* [1962], *Weber and Barrick* [1977], *Barrick and Weber* [1977], and *Masuda et al.* [1979].

Note that the phase velocity of the short waves (ocean ripples), which cause the Bragg scattering of the microwaves, does not enter (1).

The peak in the product spectrum ('Bragg resonance peak') originates from a resonance of the beat wave with a cross section modulation pattern associated with a long wave. This cross section modulation pattern moves with the phase velocity of the resonant long ocean wave. In the presence of a current in the wave propagation direction, the actual phase velocity, $c_{ph} = \omega/|\hat{\mathbf{k}}|$, differs from the value calculated from the dispersion relation for still water, $c_{ph}^{(0)} = \hat{\omega}/|\hat{\mathbf{k}}|$. If the component of the current velocity V in the propagation direction of the wave is a function of depth, then one obtains to the first order for small current velocities V $(V/c_{ph}^{(0)}) \ll 1$:

$$\bar{v}(\hat{\mathbf{k}}) \equiv c_{ph}(\hat{\mathbf{k}}) - c_{ph}^{(0)}(\hat{\mathbf{k}}) = 2|\hat{\mathbf{k}}| \int_0^\infty V(z) e^{-2|\hat{\mathbf{k}}|z}\, dz \qquad (6)$$

This equation can be derived by applying perturbation theoretical methods [see, e.g., *Schiff,* 1955]. The first-order perturbation to the phase velocity is given by

$$\bar{v}(\hat{\mathbf{k}}) = \int_0^\infty \phi^*(\hat{\mathbf{k}})\, V(z)\phi(\hat{\mathbf{k}})\, dz \Big/ \int_0^\infty \phi^*(\hat{\mathbf{k}})\,\phi(\hat{\mathbf{k}})\, dz \qquad (7)$$

where $\phi(\hat{\mathbf{k}})$ is the eigenfunction of the particle velocity (orbital velocity) associated with the ocean surface wave of wave number $\hat{\mathbf{k}}$, and $\phi^*(\hat{\mathbf{k}})$ is its complex conjugate. Since $\phi(\hat{\mathbf{k}}) \propto \exp(-|\hat{\mathbf{k}}|z)$ [see, e.g., *Phillips,* 1966; *Kinsman,* 1965], (6) immediately follows from (7).

The total phase velocity perturbation in look direction of the antenna, $v \equiv \mathbf{v} \cdot \Delta\mathbf{k}/|\Delta\mathbf{k}|$, consists of the sum of $\bar{v}$ $(= \mathbf{v}^t + \mathbf{v}^{oc} + \mathbf{v}^d)$ and the nonlinear wave-wave interaction contribution v^{nl}. It can be experimentally determined by measuring the frequency shift of the resonance peak in the spectrum $P_{B_1 B_2^*}$ of the product signal $B_1 \cdot B_2^*$ according to (1). Since $\bar{v}(\hat{\mathbf{k}})$ represents a weighted average of the current profile $V(z)$ to a depth of the order of $(2|\hat{\mathbf{k}}|)^{-1}$, one can, in principle, determine the profile $V(z)$ by performing measurements of different wave numbers $|\hat{\mathbf{k}}|$ and by inverting (6). (Note that (6) has the form of a Laplace transform.)

In the theory of the two-frequency technique, it is usually assumed that the dependence of the cross section modulation on the long ocean waves can be described by a linear transfer function. However, it is questionable whether a linear description of the scattering process is applicable at low depression angles, especially for high sea states. Therefore, second- and higher-order effects should be included in the description of the modulation.

Nonlinearities in the modulation, as well as in the wavefield, lead to higher-order contributions in the spectrum $P_{B_1 B_2^*}$. In particular, a (continuous) second-order Doppler spectrum arises from the interaction of the beat wave with two modulation patterns satisfying the second-order Bragg condition. It is expected that in the second-order spectrum, peaks evolve at $(2)^{1/2}$ times the first-order resonance frequency (for $V = 0$). Physically, such peaks can be explained as being associated with a modulation pattern of twice the resonance wavelength $\hat{\lambda}$, which propagates with a phase speed of $c_{ph}(2\hat{\lambda}) = (2)^{1/2} c_{ph}(\hat{\lambda})$.

3. THE EXPERIMENT

During the 1979 Marsen experiment, measurements with an L band pulsed two-frequency microwave scatterometer (2FS) were carried out from the Forschungsplattform Nordsee in the North Sea (54°42.0′N, 7°10.0′E). The main aim of this experiment was to test the performance of the two-frequency pulsed L band microwave scatterometer for measuring surface currents. In total, about 200 hr of data were collected during the period from September 18 to October 15, 1979. Measurements were carried out under a variety of wave and wind conditions. The significant wave height $(H_{1/3})$ varied from 0 to 3 m, and the wind speed measured at a platform height of 40 m varied from 0 to 25 m s^{-1} (0–50 kt). The geometry of the experiment is shown in Figure 1.

3.1 *The instrument*

The two-frequency L band microwave scatterometer was built by Dornier System (Germany) for the German Aerospace Research Establishment

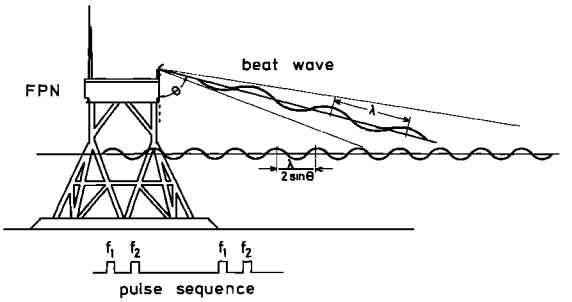

Fig. 1. Geometry of the experiment. FPN is the Forschungsplattform Nordsee (Research Platform North Sea).

(Deutsche Forschungs und Versuchsanstalt für Luft-und Raumfahrt (DFVLR)), and it was delivered in 1976. It is designed to operate from both fixed platforms and aircraft, and it therefore allows a large range of parameter settings.

The scatterometer is a pulsed system that emits successive pairs of microwave bursts of frequencies f_1 and f_2, with a time separation between pulses, which can be varied between 33 and 500 ns. One frequency, f_1, is fixed at 1320 MHz, and the other, f_2, is variable between 1260 and 1319.5 MHz. The fixed frequency is generated from a quartz oscillator of 110 MHz by frequency multiplication. The variable frequency is generated in a synthesizer, which receives a 115.333-MHz signal from a second quartz and can be switched in steps of 1/24 MHz between 109.958 and 105.000 MHz.

The modulus and phase of the backscattered signals are recorded separately on a 1-KHz carrier frequency (video frequency). The parameters of the scatterometer are summarized in Table 1. The antenna is a 37-element planar dipole array of 1.1-m diameter. It forms a circular beam with a 13° half-power beamwidth. Mechanical rotation of the antenna is used to change between HH and VV polarization. Side lobe attenuation is better than 20 dB.

3.2 *Parameters of the experiment*

The antenna was mounted on the platform at a height of 27 m above mean sea level. The measurements reported in this paper were carried out using vertical polarization of both transmitted and received signals because of the higher signal return relative to the horizontal polarization setting. The depression angle of the antenna was 4°. The duration

TABLE 1. System parameters of the L band two-frequency pulsed microwave scatterometer.

Parameter	Value
Fixed frequency	1320 MHz
Variable frequency	1260–1319.5 MHz
Frequency steps	0.5 MHz
Range of difference frequencies	0.5–50 MHz
Pulse length	Variable between 33 ns and 8.5 μs
Time separation between bursts with frequencies f_1 and f_2	Variable between 33 ns and 500 ns
Range gatings	120 m–10 km, in steps of 5 m
Pulse repetition frequency (prf)	Variable between 25 and 200 KHz
Pulse rise time	10 ns
Noise level of receiver	4 dB
Power supply	28 V dc ± 2 V, maximum 8 A
Power (effective)	50 W
Polarization	VV and HH
Weight	30 kg

of the emitted pulses and the widths of the time gates were chosen to be equal, and they varied between 600 and 1000 ns. This corresponds to a footprint radial extent ranging from 180 to 300 m. The azimuthal extent was between 115 and 180 m, as determined by the antenna beamwidth of 13° and the range from 500 to 800 m. The footprint scales were chosen as a compromise between the requirement of a high signal-to-noise ratio, which is proportional to the inverse of the footprint area, and a high resolution of the resonant line, which is proportional to the radial extent of the footprint [see *Alpers and Hasselmann,* 1978]. The difference frequencies varied between 6 and 8 MHz, corresponding to 'Bragg scattering' ocean waves with wavelengths of 25 and 18.75 m. The azimuth angle of the antenna was varied from 220° to 340°N. The predominant flow direction of the tide in this area of the North Sea is parallel or antiparallel to 300°N.

3.3 *Signal processing*

The signal processing was carried out in real time on the platform. The two signals from the video output of the 2FS were multiplied by a hardware multiplier and low-pass filtered with a cutoff frequency of 1.0 Hz. This product signal was then sampled at 2 Hz by a Hewlett-Packard HP 1000C

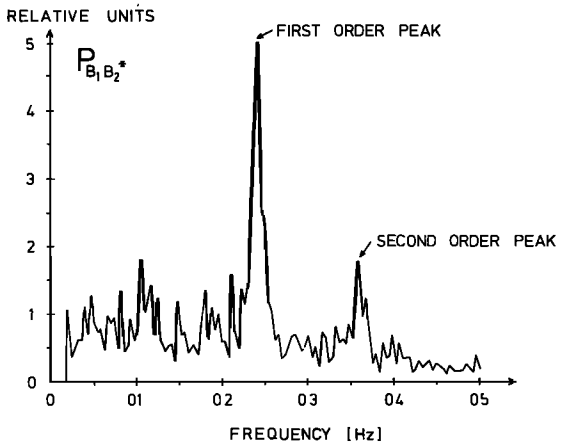

Fig. 2. Typical Doppler spectrum of the product signal $B_1 B_2^*$. Parameters: Δf = 6 MHz; VV polarization; pulse length, 990 ns; frequency resolution, 0.004 Hz; number of spectral estimates, 7; radar look direction, 325°N; wind direction, 105°N; and measurement from October 7, 1979: 5:35 h–6:23 h GMT.

Fourier analyser and stored on disc. To obtain the power spectrum of the product signal, the series was divided into segments of 256-s duration. A Hanning time window was applied to the data, and the power spectrum was calculated to a resolution of 0.004 Hz. Between five and eight such spectra were averaged, corresponding to a total record time of 21–34 min. The first-order resonance peak frequency was determined as the centroid of all spectral points within the half-power width of the peak. The phase velocity was then obtained by dividing this center frequency by the Bragg wave number of the scattering ocean wave.

3.4 *Experimental results*

Pronounced first-order resonance peaks in the Doppler spectra of the product signal, $B_1(t) \cdot B_2^*(t)$, were observed at the expected frequencies. An example is shown in Figure 2. A second-order peak on the right-hand side of the first-order resonance peak can also be seen, as is seen in many other spectra measured. Its location is at a frequency close to $(2)^{1/2}$ times the first-order resonance frequency. Furthermore, another second-order peak also seems to be visible on the left-hand side at 0.11 Hz. Such peaks occur less often than the second-order peaks on the right-hand side. Their location on the frequency axis varies considerably. Figures 3*a*, 4*a*, 5*a*, and 6*a* show time series of currents inferred from the first-order spectral peak frequencies over 15, 12, 14, and 11 hr, respectively. Positive velocities are away from the antenna. The look direction of the antenna and the wind vector are shown in Figures 3*c*, 4*c*, 5*c*, and 6*c*. The solid and dotted lines show the components of the current velocity in the look direction of the antenna, measured by the Deutsches Hydrographisches Instituts with Aanderaa current meters at a depth of approximately 9 m (v^{9m}) and 23 m (v^{23m}) (approximately 6 m above the seafloor), respectively.

The current meters were moored in a subsurface rig with a self-buoyant current meter at a 9-m depth and at a site approximately 1 km west of the platform. Figures 3*b*, 4*b*, 5*b*, and 6*b* show the difference between the velocities measured by the

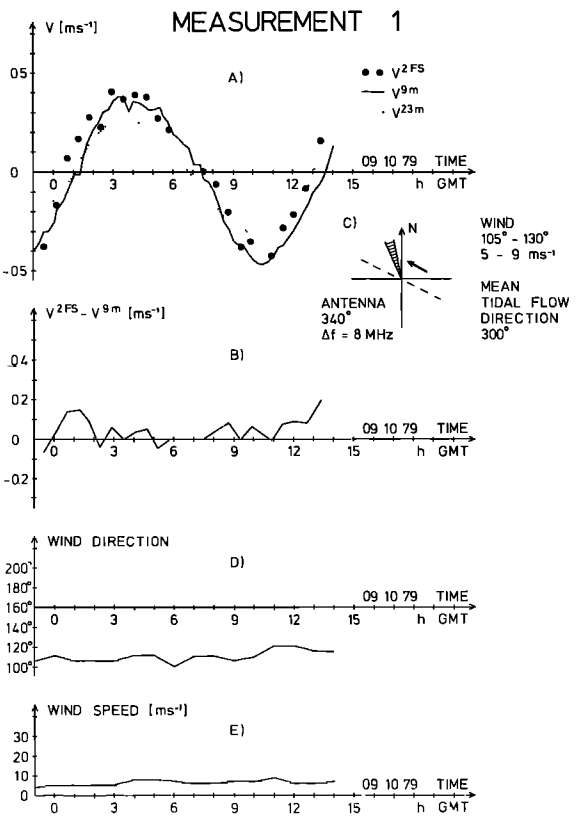

Fig. 3. (*a*) Comparison between the current velocities measured by the 2FS (closed circles) and conventional current meters at depths of 9 m (solid line) and 23 m (dotted line) for measurement 1 (October 8–9, 1979, 23:00 h–14:00 h GMT). (*b*) Difference between the velocities measured by the 2FS and the conventional current meter at 9-m depth. (*c*) Antenna look direction and wind vector measured at a height of 40 m. (*d*) Wind direction as a function of time. (*e*) Wind speed as a function of time.

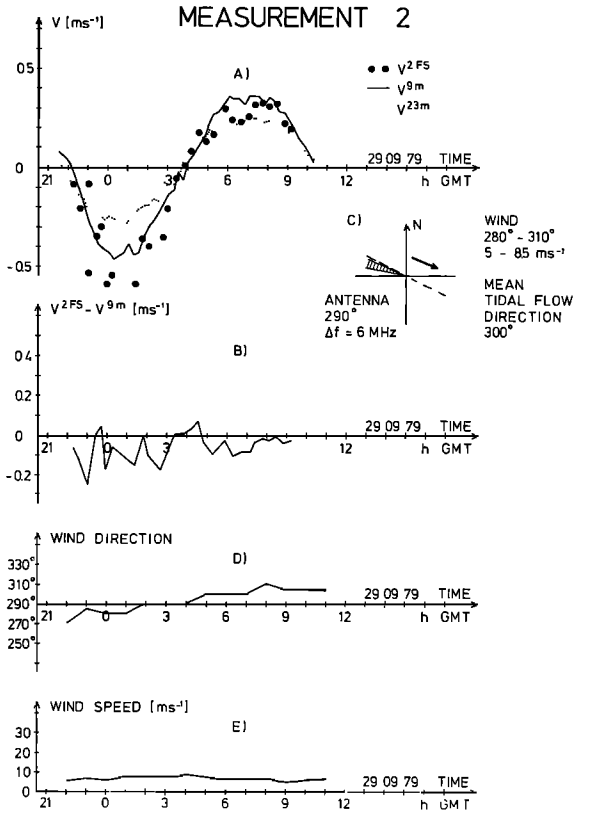

Fig. 4. Same as Figure 3, but for measurement 2 (September 28–29, 1979, 22:00 h–10:30 h GMT).

2FS and by the current meter located 9 m below the sea surface. Finally, parts *d* and *e* of the Figures 3–6 show the wind vector measured at a height of 40 m at the platform.

4. DISCUSSION

Measurements 1 and 2 were carried out under moderate wind conditions, and measurements 3 and 4, under high wind conditions.

For measurement 1 (Figure 3) the time variations of the currents measured by the 2FS and the current meter at 9 m show good agreement. The current velocity measured by the current meter at 23 m is smaller, probably because of bottom friction. The time-averaged data show a slight difference (0.06 m s^{-1}) between v^{2FS} and v^{9m}. The fluctuations around this mean value lie within the expected error bars.

Measurement 2 shows the same general features as measurement 1. This is a case where the wind direction is approximately antiparallel to the antenna beam ('upwind'), whereas for the other three measurements reported here the antenna beam is approximately 'downwind.' A significant deviation of the 2FS from the 9-m velocity occurs when the wind is parallel to the flow direction. This is interpreted as a wind effect and will be discussed below.

Measurement 3 shows the influence of strong winds on the surface current in the uppermost layer of the ocean. A strong wind-induced surface drift is measured by the 2FS superimposed on the tidal cycle, as measured by the two in situ current meters. The surface drift appears to be significantly augmented when the tidal flow and wind directions are oriented approximately parallel, but the surface drift is small when they are approximately antiparallel. This could be explained by a strong interaction of the tidal current with the wind-induced current due to a large current shear. The mean of $v^{2FS} - v^{9m}$ over the whole tidal cycle is 0.28

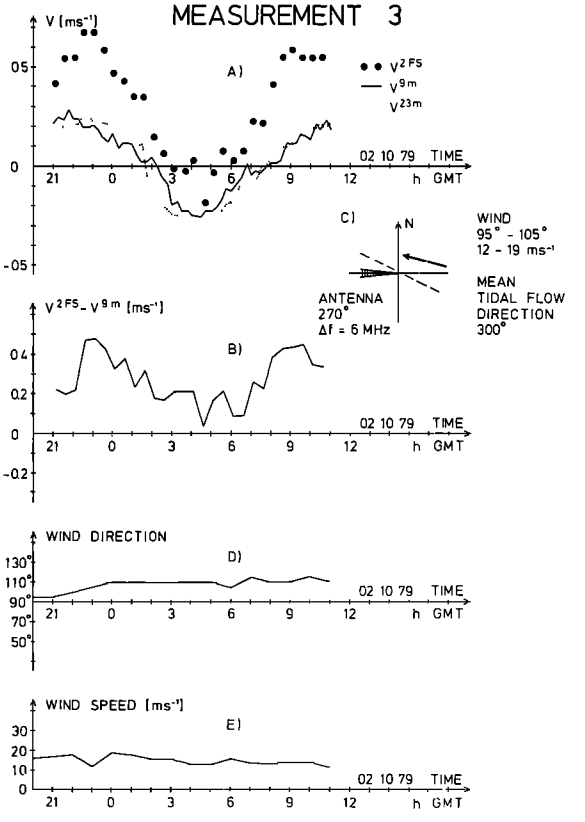

Fig. 5. Same as Figure 3, but for measurement 3 (October 1–2, 1979, 21:00 h–11:00 h GMT).

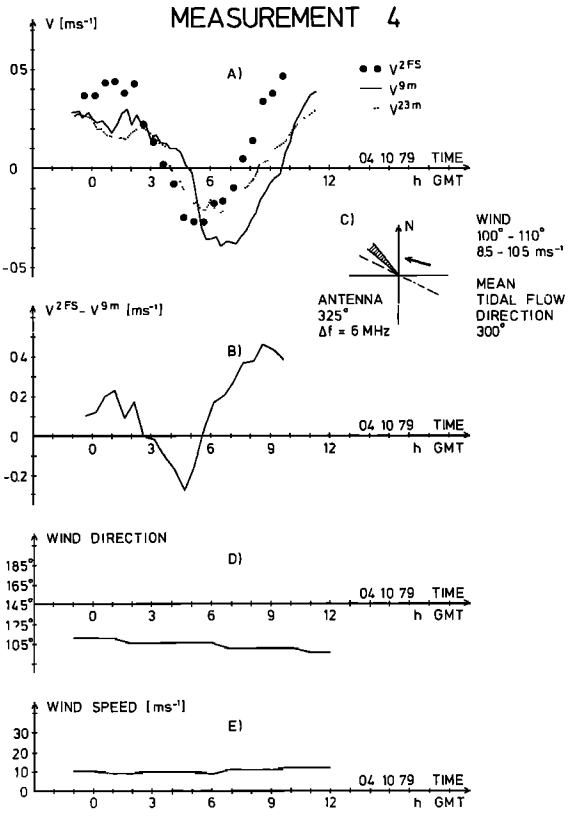

Fig. 6. Same as Figure 3, but for measurement 4 (October 3–4, 1979, 22:30 h–10:30 h GMT).

m s^{-1}. The velocity gradient between the in situ measurements at 9- and 23-m depths is very small. We interpret this as a consequence of the strong wind-induced turbulent mixing, leading to a deepening of the wind-mixed layer.

Measurement 4 is also a high wind case, showing the effect of winds on the current in the uppermost layer of the ocean. However, in contrast to measurement 3, this measurement shows very large variations in the current shear. We do not attribute the data points obtained by the 2FS to errors in the measurement but they are an indication of additional information not contained in the in situ current meter records. Indeed, large current shears are not unexpected in the German Bight, as shown by model calculations of *Backhaus* [1980]. The local current velocity at a given depth is determined by many factors, for example, by tidal forces, wind stress, bottom friction, and basin configurations, which give rise to transient features such as inertial oscillations and seiches. In this paper, we do not attempt to interpret the current records oceanographically, since the time series of the 2FS measurement is too short to derive decisive conclusions about the physical mechanism causing the large variations in the vertical current shear. In order to answer these questions, continuous two-dimensional current measurements over several tidal cycles with fixed parameter settings are required.

5. ERROR ANALYSIS

The accuracy of the current measurements depends on the accuracy of the measurement of the centroid of the resonant peak and on the accuracy with which $\hat{f}$ and $\hat{\mathbf{k}}$ can be calculated. The finite extent L of the footprint implies an indeterminacy in the wave number $\hat{\mathbf{k}}$ of the Bragg ocean wave of the following order:

$$|\delta\hat{\mathbf{k}}| = \frac{\alpha}{L} \tag{8}$$

where α is a numerical factor, which depends on the antenna pattern. (For a Gaussian antenna pattern, $\alpha = 2.35$ if L is defined by the 6-dB point.) The indeterminacy of $\hat{\mathbf{k}}$ implies an indeterminacy of the phase velocity $c_{ph} = (g/|\hat{\mathbf{k}}|)^{1/2}$ (for simplicity, we assume that $d = \infty$), given by

$$\frac{\delta c_{ph}}{c_{ph}} = \pm\frac{1}{2}\left|\frac{\delta\hat{\mathbf{k}}}{\hat{\mathbf{k}}}\right| \tag{9}$$

In our measurements $|\delta\hat{\mathbf{k}}/\hat{\mathbf{k}}|$ is less than 0.026, which results in an error in the phase velocity of $\delta c_{ph} = 0.07 - 0.08$ m s^{-1}.

The frequency of the resonance peak is resolved in frequency bands of 0.004-Hz width, because the length of the time segments used for calculating the Doppler spectrum is 256 s. This results in an error for determining the phase velocity, which is given by

$$\delta c_{ph} = \pm\pi|\hat{\mathbf{k}}|^{-1}\delta f \tag{10}$$

Inserting $|\hat{\mathbf{k}}|^{-1} = (2\pi)^{-1} \cdot 25$ m and $(2\pi)^{-1} \cdot 18.75$ m yields $|\delta c_{ph}| = (0.04 - 0.05)$ m s^{-1}. In principle, this error can be reduced by increasing the segment length for calculating the Doppler spectra. However, in this case, the number of degrees of freedom for the spectral estimate decreases if the total record length is kept constant. Consequently, the probability for detecting the resonance peak in the background decreases.

By adding the two errors arising from the finite

footprint size and the frequency resolution, we obtain the following system errors in the surface velocity for our experiment:

$$(\delta c_{ph})^{total} = \pm(0.11 - 0.13)\ m\ s^{-1} \quad (11)$$

Another error arises through the finite averaging time required for the measurement. The surface current varies in this area of the North Sea, with a maximal velocity change of approximately 0.2 $m\ s^{-1}/hr$. If the time-averaging error is to be kept smaller than the error arising from the radial extent of the footprint, then the integration time is limited to about 30 min.

6. CONCLUSIONS AND OUTLOOK

The measurements clearly show the usefulness of the two-frequency scatterometer for measuring ocean surface currents from fixed platforms in real time. The technique yields the current in the upper few meters of the ocean, which is strongly influenced by the action of the wind stress. In conjunction with in situ current measurements at greater depth, this technique is an ideal research tool for investigating the transfer of horizontal momentum from wind to water. The technique described here can be extended to provide measurements of the two-dimensional surface current vector by installing two antennae with azimuthal angles 90° apart. In comparison with the HF techniques, an advantage of the 2FS microwave technique is that it operationally needs only small antennae, relatively simple electronics, and simple processing. A disadvantage is its smaller range. Furthermore, interferences with signals from radio stations do not limit its application. Another advantage of the two-frequency technique is that it is relatively easy to sweep the complete surface wave spectrum and thus obtain vertical current shear information. In conclusion, we believe that this technique ideally complements the HF technique for measuring ocean surface currents.

Acknowledgments. We thank Professor K. Hasselmann for many stimulating discussions. This work was supported in part by the German Science Foundation (DFG-SFB 94, Schwerpunktprogramm Fernerkundung). MARSEN contribution 1.

REFERENCES

Alpers, W., and K. Hasselmann (1978), The two-frequency microwave technique for measuring ocean wave spectra from an airplane or satellite, *Bound. Layer Meteorol., 13,* 215–230.

Backhaus, J. O. (1980), Simulation von Bewegungsvorgängen in der Deutschen Bucht, *Dt. Hydrograph. Z., Ergänzungsheft, B, 14.*

Barrick, D. E. (1978), HF surface-current mapping radar 1977 Alaskan Operations–Lower Cook Inlet, *Prelim. Rep.*, Wave Propagat. Lab., Natl. Oceanic Atmos. Adm., Boulder, Colo.

Barrick, D. E., and B. L. Weber (1977), On the nonlinear theory for gravity waves on the ocean's surface, Part 2. Interpretation and Applications, *J. Phys. Oceanogr., 7,* 11–21.

Barrick, D. E., M. W. Evans, B. L. Weber (1977), Ocean surface currents mapped by radar, *Science, 198,* 138–144.

Ha, E.-C. (1979), Remote sensing of ocean surface current and current shear by HF backscattering radar, *Tech. Rep. D415-1,* Cent. for Radar Astron., Stanford Electron. Lab., Stanford Univ., Stanford, Calif.

Kinsman, B. (1965), *Wind Waves,* pp. 117–144, Prentice-Hall, Englewood Cliffs, N. J.

Longuet-Higgins, M. S., and O. M. Phillips (1962), Phase velocity effects in tertiary wave interactions, *J. Fluid Mech., 12,* 333–336.

Masuda, A., Y. J. Kuo, and H. Mitsuyasu (1979), On the dispersion relation of random gravity waves, Part 1. Theoretical framework, *J. Fluid Mech., 92,* 717–730.

Phillips, O. M. (1966), *The Dynamics of the Upper Ocean,* pp. 22–23, Cambridge Univ. Press, New York.

Plant, W. J. (1977), Studies of backscattered sea return with CW dual-frequency, X-band radar, *IEEE Trans. Antennas Propagat., AP-25,* 28–36.

Schiff, I. (1955), *Quantum Mechanics,* pp. 151–176, McGraw-Hill, New York.

Schuler, D. L. (1978), Remote sensing of directional gravity wave spectra and surface currents using a microwave dual-frequency radar, *Radio Sci., 13,* 321–331.

Stewart, R. H., and J. W. Joy (1974), HF radio measurements of surface currents, *Deep Sea Res., 21,* 1039–1049.

Teague, C. C., G. L. Tyler, and R. H. Stewart (1977), Studies of the sea using HF radio scatter, *IEEE Trans. Antennas Propagat., AP-25,* 12–19.

Weber, B. L., and D. E. Barrick (1977), On the nonlinear theory for gravity waves on the ocean's surface, Part 1. Derivations, *J. Phys. Oceanogr., 7,* 3–10.